Nov 7th, 12:00 AM - Nov 8th, 12:00 AM

Experimental Study on Uplift Capacity of Purlins considering Restraints from Standing Seam Roof Systems

Wei Luan

Yuanqi Li

Wei-Wen Yu International Specialty Conference on Cold-Formed Steel Structures
St. Louis, Missouri, U.S.A., November 7 & 8, 2018

Experimental study on uplift capacity of purlins considering restraints from standing seam roof systems

Wei Luan[1], Yuanqi Li[2]*

Abstract

A total of 32 specimens of single-span purlin roof assemblies considering uplift wind load were tested to investigate the structural behavior of cold-formed steel purlins with one flange fastened to standing seam roofs. Failure modes and failure loads of purlins with different parameters were obtained. Full finite element models, incorporate purlins, clips and standing seam roof panels, were developed, and the analysis results were consistent to a high degree with the test results. Using the same element type and material model, the rotational restraint of test roof systems and corresponding influence factors were investigated by finite element models. Finally, using the rotational restraint rigidities and comparing with the test results, the lateral restraint of test roof systems were also studied through a simple finite element model incorporates pure the purlin and presents the rotational restraints and lateral restraints by rotational and lateral springs. It is shown that the standing seam roofs do provide some extent of rotational restraints and lateral restraints to purlins at the connection points, especially for purlins without sag rod.

[1] Department of Structural Engineering, Tongji University, Shanghai 200092, China
[2] State Key Laboratory of Disaster Reduction in Civil Engineering, Shanghai 200092, China
Corresponding author at: Department of Structural Engineering, School of Civil Engineering, Tongji University Shanghai 200092, China.
Email: liyq@tongji.edu.cn

Keywords

cold-formed steel purlins; standing seam roof system; uplift capacity; lateral restraints; torsional restraints; bending bearing capacity

Introduction

Cold-formed C- and Z-purlins are widely used in metal buildings due to their economy, ease of fabrication, and high strength-to-weight ratios. However, these sections are weak in the lateral direction and in torsion. Previous work shows that conventional roof panels which are directly through-fastened to the purlins by self-tapping screws can provide full lateral bracing and some extent of torsional restraint to the purlins by virtue of their shear rigidity and resistance to local bending at the connections[1-3]. In recent years, standing seam roof systems are very prevalent since they are well adapted to the thermal expansion and contraction deformation caused by temperature changes. In these roof systems, the roof panel are attached to the purlins with clips, through which the movement of the purlins relative to the roof panels is permitted. Therefore the behavior of purlins in these roof systems lies in between full lateral support and no lateral support. An experimental procedure used for determining system strength under gravity loading has been proposed by Murray et al. [4-6]. The procedure is referred to as the "base test method" and uses the results of single span tests to predict the capacity of continuous muti-span systems. Based on eight rows of single span and three-span tests, Anderson [7] proved that for uplift loading the failure load of a multi-span standing seam roof system can not be effectively and accurately predicted by the base test method, a reduction factor for the base test method and a lap length modification were proposed. Fisher and Nunnery [8] investigated the effects of the diaphragm on base test results through several tests, and found that an average increase in strength of 32 percent occurred when the edge angle was used in the base test. Trout [9] investigated the possibility of eliminating some of the roof system parameters

from the required test matrix, and found that clip type, purlin flange width, and roof panel thickness all have an effect on the strength of standing seam roof systems, none of the roof components can be completely eliminated.

Because of the variety of the deck profile, standing seam configuration and clip details in standing seam roof systems, it is difficult to develop analytical methods to predict the strength of purlins attached to them. Thus in this paper the uplift capacity of Z-and C-purlins supporting standing seam roof systems were studied through 32 tests, and the rotational restraints and torsional restraints provided by two test standing seam roof systems were investigated using finite element models.

Experimental Investigation

Test Specimens

Representative standing seam roof systems from two different manufactures were used for the tests. These were LSⅢ sheeting with LS003 clip and SS360 sheeting with S3PC-1 clip as shown in Fig. 1 and Fig. 2. Z-purlins and C-pulins were used in the tests with the depth, flange width and thickness varied. Each test specimen consists of a type of standing seam roof system and four Z-purlins spaced 1.2m or three C-purlins spaced 1.5m. All the Z- and C-purlins were 7.2m in length and their flanges face to the same direction. Sag rods were used in some test specimens with location at middle point or third points, as shown in Fig. 3. Standard two-hole cleats were used for all tests except test Z20322-L-0S, in which only one bolt was installed at the lower hole with the upper hole attaching to a sag rod. With a repeat specimen designed for each test, a total of 32 specimens were tested, the configuration details of test specimens are given in Table 1.

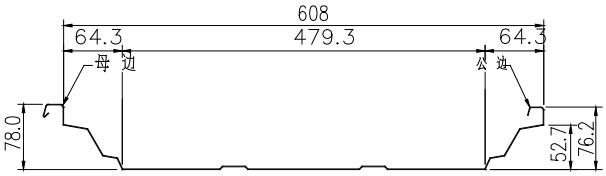

Figure 1. Representative configuration of LSⅢ sheeting and LS003 clip

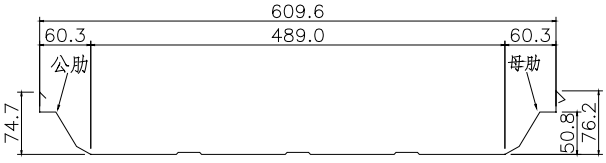

Figure 2. Representative configuration of SS360 sheeting and S3PC-1 clip

Figure 3. Sag rod configuration

Table 1: Configuration details of test specimens

Test identification	Purlin shape	Purlin Depth (mm)	Purlin Width (mm)	Purlin Thickness (mm)	roof type	Bracing points
Z20322-L-0	Z	203	64	2.2	LSⅢ	
Z20379-L-0	Z	203	79	2.2	LSⅢ	
Z23322-L-0	Z	233	64	2.2	LSⅢ	
Z20322-L-1	Z	203	64	2.2	LSⅢ	Middle
Z20322-L-2	Z	203	64	2.2	LSⅢ	Third

Z20315-S-0	Z	203	64	1.5	SS360	
Z20322-S-0	Z	203	64	2.2	SS360	
Z20322-S-1	Z	203	64	2.2	SS360	Middle
Z20322-S-2	Z	203	64	2.2	SS360	Third
Z20322-L-0S	Z	203	64	2.2	LSIII	
C20316-L-0	C	203	65	1.6	LSIII	
C20320-L-0	C	203	65	2.0	LSIII	
C20325-L-0	C	203	65	2.5	LSIII	
C25420-L-0	C	254	65	2.0	LSIII	
C20320-L-1	C	203	65	2.0	LSIII	Middle
C20320-L-2	C	203	65	2.0	LSIII	Third

Test Rig and Operation

The tests were conducted mainly with reference to the procedures outlined in AISI S908-13 'Base Test Method for Purlins Supporting a Standing Seam Roof System'. The simulated wind uplift loading was applied by means of a test chamber, which was 7.4m in length, 4.5m in width, 0.6m in height and made of shaped steel and steel plates. The purlins were placed inside the test chamber, and the roof panels were installed over the purlins. To provide an airtight seal over the test assembly, the chamber was covered with a continuous piece of 0.15 mm polyethylene sheeting between the purlins and roof panels as shown in Fig. 4.

Figure 4. Fully assembled roof system on test rig with plastic sheeting

A motor driven blower was used to inflate the chamber so that the effect of uniform upward pressure was acted on the roof system. Vertical displacement (δ_v) and horizontal displacement (δ_{hb}) at the intersection of the web and the bottom flange in the middle span of purlins, horizontal displacement (δ_{hu}) at the intersection of the web and the upper flange in the middle span of purlins, the strains of the bottom flange in the longitudinal direction at the middle span of central purlins, and the pressure (P) in the test chamber were measured and recorded.

Test Results

In general, the failure modes of Z-purlins and C-purlins in the tests were nearly the same and mainly related to the number of sag rods being used. For tests without sag rods, the failure of purlins generally took place near the mid span and with an apparent local buckling at the web to bottom flange junction after considerable lateral movement, as shown in Fig. 5. For tests with one row of sag rods, the failure mode of purlins was buckling of lip stiffener and distortional buckling of lip and bottom flange adjacent to the location of sag rods, as shown in Fig. 6. For tests with two rows of sag rods, the failure mode of purlins was buckling of lip stiffener and distortional buckling of lip and bottom flange near the third points of purlins, with local buckling at the web to bottom flange junction occurred near the mid span simultaneously, as shown in Figure 7.

(a) Considerable lateral movement of Z-purlin and C-purlin

(b) Local buckling of Z-purlin and C-purlin

Figure 5. Failure modes of Z-purlin and C-purlin without sag rods

Figure 6. Failure modes of Z-purlin and C-purlin with one row of sag rods

Figure 7. Failure modes of Z-purlin and C-purlin with two rows of sag rods

Typical load-displacement curves of Z-purlins and C-purlins are plotted in Fig. 8~10. For purlins without sag rods, the curves are initially linear and shows prominent nonlinearity as the load increases. For purlins with one row or two rows of sag rods, the curves stay linear until lip buckling and local buckling occurs.

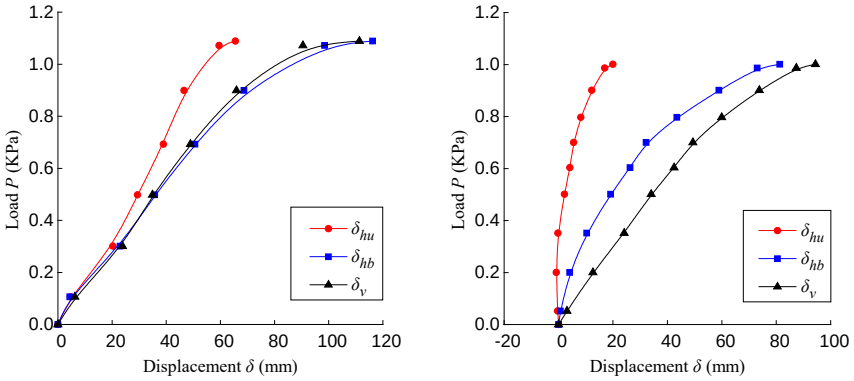

(a) curve of Z20322-L-0 (b) curve of C20320-L-0

Figure 8. Typical load-displacement curves of purlins without sag rods

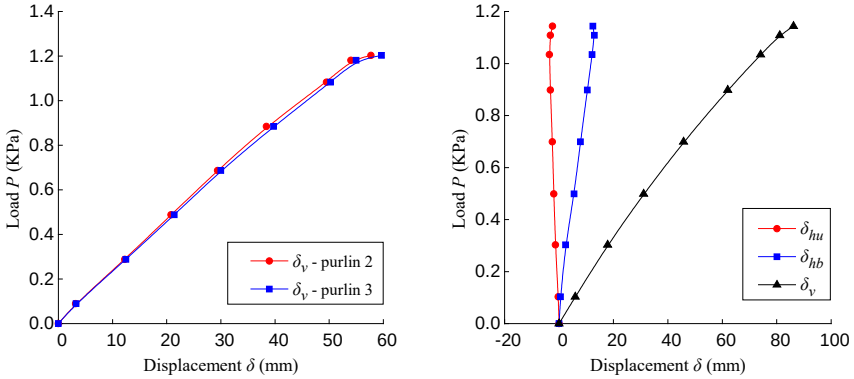

(a) curve of Z20322-L-1 (b) curve of C20320-L-1

Figure 9. Typical load-displacement curves of purlins with one row of sag rods

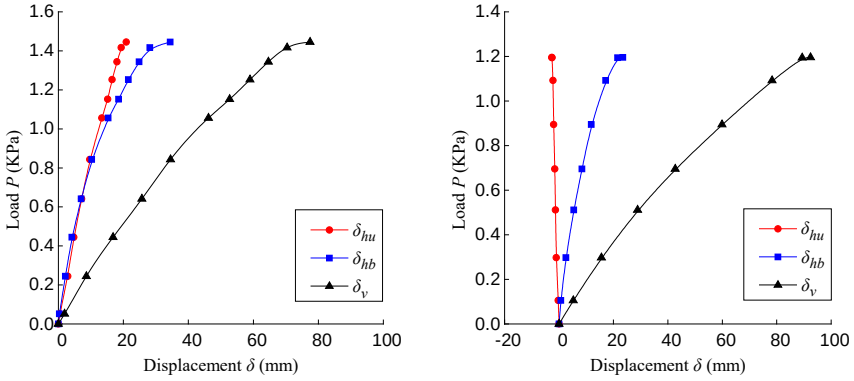

(a) curve of Z20322-L-2 (b) curve of C20320-L-2

Figure 10. Typical load-displacement curves of purlins with two rows of sag rods

The failure load (P_u) and corresponding bending bearing capacity (M_{ts}) of Z-purlin tests and C-purlin tests are summarized in Table 2 and 3. For each given test, the reduction factor (R_t) was also calculated according to AISI

S908-13. The reduction factors of C-purlins are generally greater than that of Z-purlins, especially for tests with one row or two rows of sag rods. For tests without sag rods, the reduction factors are also related to the flange width, depth and thickness of the purlins. The nominal flexural strength (M_{ne}) for global (lateral-torsional) buckling calculated using the relevant sections of AISI S100 F2[10], the bending bearing capacity (M_{GB}) calculated using Chinese Code (GB50018)[11], and the test flexural capacity (M_{ts}) of purlins are compared and presented in table 4. The material properties of purlins acquired through tensile coupon tests are used in calculating both of the design strengths. For purlins without sag rods, both the nominal flexural strength and bending bearing capacity for global (lateral-torsional) buckling calculated using the AISI specification and Chinese Code are overly conservative, because the considerable torsional and lateral restraints provided by the standing seam roof systems are not considered. For purlins with one row or two rows of sag rods, both of the specification calculated results are smaller than the test results， except for Z-purlins with two rows of sag rods, the test results are slightly smaller, which means the lateral deflection of the purlin at bracing points may not be effectively restrained by the sag rods.

Table 2: Test results of Z-purlin specimens

Test specimen identification	Failure load P_u (kN/m^2)	Self weight P_d (kN/m^2)	Tributary width of purlin S (m)	Failure load on purlin w_{ts} (kN/m)	Test flexural strength M_{ts} (kNm)	Flexural strength M_{nt} (kNm)	R_t (M_{ts}/M_{nt})
Z20322-L-0	1.211	0.116	1.200	1.314	8.51	14.52	0.586
Z20322-L-0R	1.204	0.116	1.200	1.3056	8.46	14.52	0.583
Z20322-L-0S	1.188	0.116	1.200	1.2864	8.34	14.52	0.574
Z20322-L-0SR	1.202	0.116	1.200	1.3032	8.44	14.52	0.581
Z20379-L-0	1.416	0.119	1.200	1.5564	10.09	15.17	0.665
Z20379-L-0R	1.412	0.119	1.200	1.5516	10.05	15.17	0.663

Z23322-L-0	1.494	0.119	1.200	1.65	10.69	18.14	0.590
Z23322-L-0R	1.477	0.119	1.200	1.6296	10.56	18.14	0.582
Z20315-S-0	0.910	0.099	1.200	0.9732	6.31	9.83	0.641
Z20315-S-0R	0.894	0.099	1.200	0.954	6.18	9.83	0.629
Z20322-S-0	1.205	0.116	1.200	1.3068	8.47	14.52	0.583
Z20322-S-0R	1.184	0.116	1.200	1.2816	8.30	14.52	0.572
Z20322-L-1	1.319	0.116	1.200	1.4436	9.35	14.52	0.644
Z20322-L-1R	1.333	0.116	1.200	1.4604	9.46	14.52	0.652
Z20322-S-1	1.288	0.116	1.200	1.4064	9.11	14.52	0.628
Z20322-S-1R	1.252	0.116	1.200	1.3632	8.83	14.52	0.608
Z20322-L-2	1.613	0.116	1.200	1.7964	11.64	14.52	0.802
Z20322-L-2R	1.561	0.116	1.200	1.734	11.24	14.52	0.774
Z20322-S-2	1.581	0.116	1.200	1.758	11.39	14.52	0.784
Z20322-S-2R	1.556	0.116	1.200	1.728	11.20	14.52	0.771

The last letter R of the specimen identification represents the repeat test specimen for corresponding test.

Table 3: Test results of C-purlin specimens

Test specimen identification	Failure load P_u (kN/m^2)	Self weight P_d (kN/m^2)	Tributary width of purlin S (m)	Failure load on purlin w_{ts} (kN/m)	Test flexural strength M_{ts} (kNm)	Flexural strength M_{nt} (kNm)	R_t (M_{ts}/M_{nt})
C20316-L-0	0.859	0.092	1.500	1.151	7.46	10.61	0.702
C20316-L-0R	0.850	0.092	1.500	1.137	7.37	10.61	0.694
C20320-L-0	1.102	0.101	1.500	1.502	9.73	13.47	0.722
C20320-L-0R	1.106	0.101	1.500	1.508	9.77	13.47	0.725
C20325-L-0	1.333	0.110	1.500	1.835	11.89	20.80	0.571
C20325-L-0R	1.360	0.110	1.500	1.875	12.15	20.80	0.584
C25420-L-0	0.911	0.106	1.500	1.208	7.82	19.28	0.406
C25420-L-0R	0.906	0.106	1.500	1.200	7.78	19.28	0.403

C20320-L-1	1.245	0.101	1.500	1.716	11.12	13.47	0.825
C20320-L-1R	1.202	0.101	1.500	1.652	10.70	13.47	0.794
C20320-L-2	1.297	0.101	1.500	1.794	11.63	13.47	0.863
C20320-L-2R	1.295	0.101	1.500	1.791	11.61	13.47	0.861

The last letter R of the specimen identification represents the repeat test specimen for corresponding test.

Table 4: Test results of C-purlin specimens

Test identification	M_{ts} (kNm)	M_{GB} (kNm)	M_{ne} (kNm)	M_{ts} /M_{GB}	M_{ts} / M_{ne}
Z20322-L-0	8.49	2.12	1.86	4.005	4.553
Z20322-L-0S	8.39	2.12	1.86	3.960	4.501
Z20379-L-0	10.07	3.23	3.10	3.114	3.253
Z23322-L-0	10.63	2.53	2.14	4.193	4.966
Z20315-S-0	6.24	1.41	1.30	4.441	4.799
Z20322-S-0	8.39	2.12	1.86	3.958	4.499
			Mean	3.945	4.429
Z20322-L-1	9.41	7.56	8.52	1.245	1.104
Z20322-S-1	8.97	7.56	8.52	1.188	1.053
Z20322-L-2	11.44	12.09	12.11	0.947	0.945
Z20322-S-2	11.29	12.09	12.11	0.935	0.933
			Mean	1.078	1.009
C20316-L-0	7.41	1.68	1.52	4.417	4.861
C20320-L-0	9.75	2.32	1.92	4.211	5.082
C20325-L-0	12.02	3.89	2.40	3.087	5.016
C25420-L-0	7.80	3.13	2.56	2.491	3.047
			Mean	3.551	4.501
C20320-L-1	10.91	7.36	8.63	1.483	1.264
C20320-L-2	11.62	10.10	11.51	1.150	1.009
			Mean	1.317	1.137

Finite Element Analysis

The finite element program ANSYS was used to develop finite element models and perform nonlinear analysis of the test purlin roof systems subjected to wind uplift load. The finite element models incorporated purlins, clips and standing seam roof panels with the dimensions exactly the same as the test specimens.

Element Type and Mesh

The SHELL181 element, a 4-node shell element with six degrees of freedom at each node was used for modeling purlins, standing seam roof panel and clips. Based on reasonable consideration of the stress stiffening, large rotation and large strain, the SHELL181 element is well-suited for analyzing thin to moderately-thick shell structures. The sag rods were modeled using the LINK10 element, a 2-node 3-D spar element with the tension-only option. The stiffness is removed if the element goes into compression, which is in line with the actual working condition of sag rods. To simulate the contact and sliding between the base and tab of the clips, contact pairs were established using the CONTA 173 element and TARGE 170 element. The finite element mesh size of the model was investigated to provide both accurate and time-efficient results.

Material Model

Standing seam roof panels, clips and sag rods were all modeled as non-linear materials using the ideal elastic-plastic model, the yield stresses were obtained from product reports provided by the manufactures. The measured material properties of purlins obtained from the coupon tests were included in the finite element model using a mathematical model, in which the true stress and the logarithmic plastic strain were adopted. The material properties of the flat potions were also used for the round corners of the purlin sections.

Boundary Condition and Loading Condition

To model the simply supported boundary condition, at both ends of each purlin, the translation in the vertical direction of the central point and the translations in the lateral direction of the web line points were constrained. The translation in the longitudinal direction of the central point at one end of the purlin was also constrained to avoid rigid body displacement. Uniformly distributed loads vertical the bottom surface of the standing seam roof panels were applied to simulate the wind uplift load

Verification of Finite Element Models

The developed finite element models were verified against the experimental results. The load-displacement curves and failure modes predicted by the finite element analysis were compared with the test results. In general, the finite element models showed to be accurate in terms of failure load, failure mode, and load-displacement curve. Take specimen Z20322-L-0 as an example, The comparison of load-displacement curves and failure modes are shown in Fig. 11.

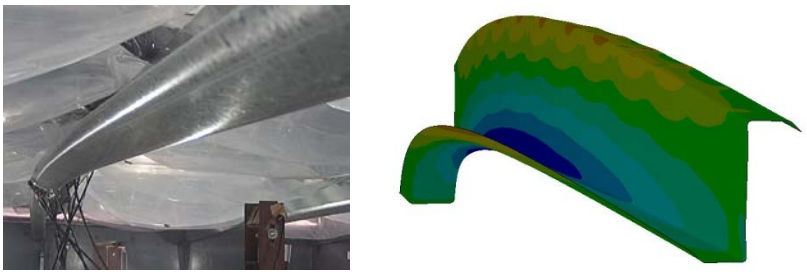

(a) Considerable lateral movement of Z-purlin

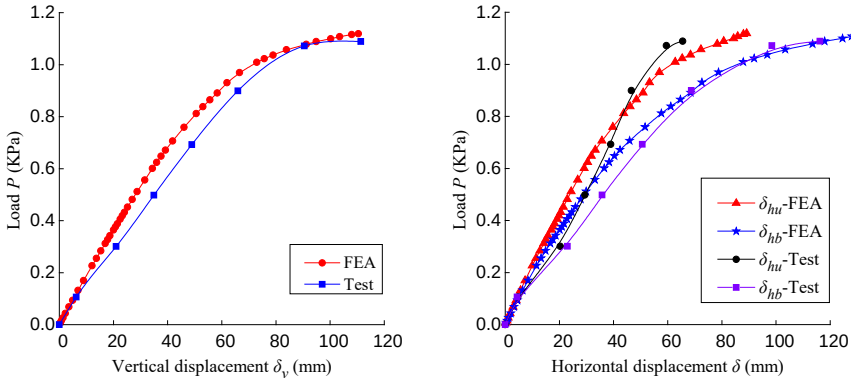

(b) load-displacement curves

Figure 11. Comparison of test results and FEA results for specimen Z20322-L-0

Rotational Restraint of Standing Seam Roof Systems

Finite Element Models

Based on the verified finite element models of the test purlin roof systems and using the same element type and material model, a finite element model used for analyzing the rotational restraint of standing seam roof systems were established as shown in Fig. 12. A pair of concentrated forces with same value and opposite direction were applied at two screw connection points of each clip base to simulate the torque transmitted from the purlin.

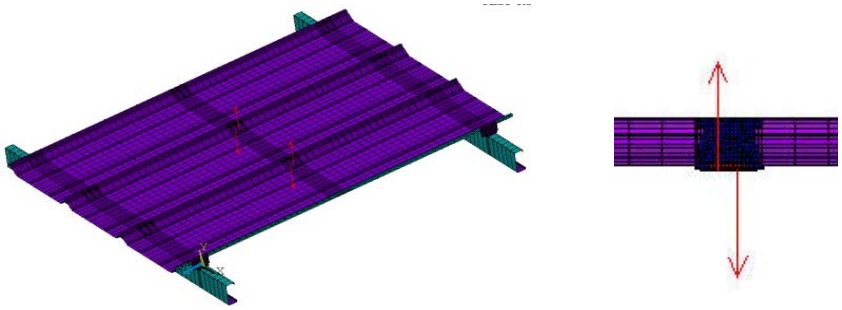

Figure 12. Finite element model for analyzing rotational restraint of standing seam roof systems

Calculation of Rotational Restraint Rigidity

Using the analysis results from the finite element model, the rotational restraint rigidity can be calculated according to Equation 1.

$$K = \frac{T}{\theta} = \frac{F \times s}{|\delta_1 - \delta_2|/s} \quad (1)$$

in which T is the torque applied at the clip base, θ is the corresponding rotation angle of the clip base, F is the concentrated force applied at the screw points, s is the space between the screws, δ_1 and δ_2 are the corresponding displacements of screw points.

The rotational restraint rigidity to unit length of purlin can be calculated according to Equation 2.

$$K_{tor} = \frac{K}{w_{rf}} \quad (2)$$

in which w_{rf} is the width of corresponding standing seam roof panel.

Analysis of Influence Factors

Using the finite element models, the influence of different factors on the rotational restraint rigidity provided by two test standing seam roof systems were studied. The variables include the relative sliding of clip tab and clip base S_{tb}, roof panel thickness t_{rf} and clip tab thickness t_{ct}. Analysis results are shown in Fig. 13. It is shown that the rotational restraint rigidity is mainly depend on the clip tab thickness, because the clip tab is the weakest link in the rotational restraint transmission path of the standing seam roof system. The roof panel thickness also has some influence but not very much, and the influence of the relative sliding of clip tab and clip base can be neglected except for LS003 clip, when the relative sliding value is larger than 40mm, half of the clip tab is

separated from the clip base, thus the rotational restraint is very small.

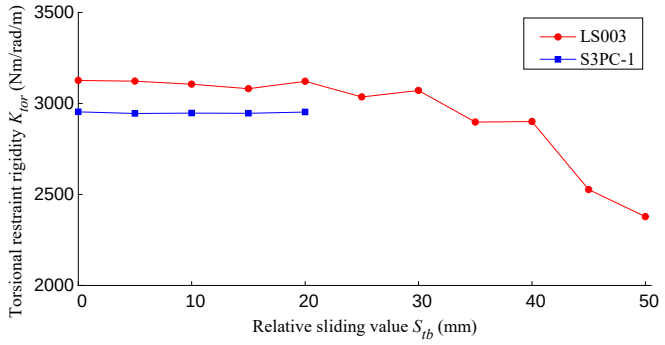

(a) Correlation between K_{tor} and S_{tb}

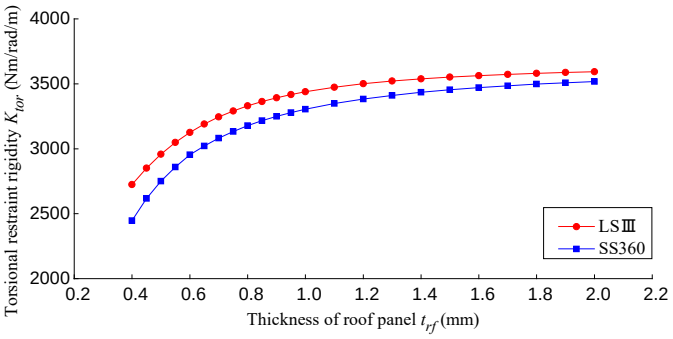

(b) Correlation between K_{tor} and t_{rf}

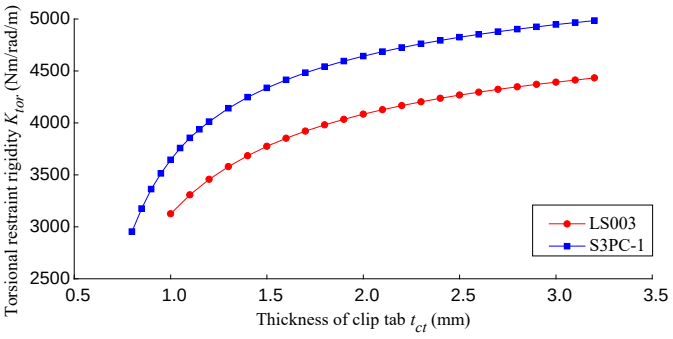

(c) Correlation between K_{tor} and t_{ct}

Figure 13. Correlation between the rotational restrain rigidity K_{tor} and factors

Lateral Restraint of Standing Seam Roof Systems

Simple Finite Element Model

The accuracy and reliability of full finite element models incorporated purlins, clips and standing seam roof panels have been verified by the test results. However, the full model required both a large amount of computer memory and considerable running time. Therefore a simple finite element model incorporated purely the purlin was then established. In the simple model, the rotational restraints and lateral restraints provided by roofs were represented by rotational and lateral springs placing at locations where the roof panels attaching to purlins through clips.

Analysis of Lateral Restraint Rigidity

Based on the rotational restraint rigidity obtained from above analysis, and through the comparison of failure modes, failure loads and load-displacement curves obtained from finite element analysis with test results, the lateral restraint rigidities provided by test roof systems were investigated. The lateral restraint rigidity of the test standing systems can be described using a mathematical model as shown in Fig. 14. The values for corresponding parameters are given in Table 5.

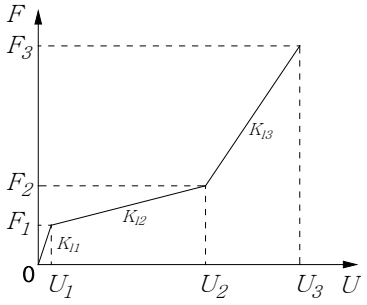

Figure 14. Model for calculation of lateral restraint rigidity

Table 5: Values of parameters

Subscript number	LSⅢ roof system			SS360 roof system		
	U (m)	F (N)	K_l (N/m/m)	U (m)	F (N)	K_l (N/m/m)
1	0.002	13	10500	0.001	31	51000
2	0.018	56	4469	0.023	224	14977
3	0.031	201	18628	0.047	700	32796

Conclusion

A total of 32 specimens of single-span purlin roof assemblies considering uplift wind load were tested. Failure modes, failure loads and load-displacement curves of Z- and C-purlins were obtained. For each given test, the reduction factor was also calculated according to AISI S908-13. The bending bearing capacity of purlins for global buckling calculated using AISI Specification (AISI S100) and Chinese Code (GB50018) were compared with the test results. In general, both of the specification calculated results are smaller than the test results, especially for purlins without sag rod, the specifications are overly conservative. Full finite element models, incorporate purlins, clips and standing seam roof panels, were developed and verified by the test results. Rotational restraint and lateral restraint provided by the standing seam roof systems were

also analyzed using simple finite element models. It is shown that the standing seam roofs do provide some extent of rotational restraints and lateral restraints to purlins at the connection points, especially for purlins without sag rod. The rotational restraint rigidity is mainly depend on the clip tab thickness.

Acknowledgements

The research was from the topic of the National Science Foundation of China (No.51478331). The authors are grateful to the financial support of the research fund of the State Key Laboratory of Disaster Reduction in Civil Engineering (No. SLDRCE14-B-06) and the authors are also grateful to USAS Building System and ABC Building Systems (China) for supplying the test specimens.

References

[1] Peköz T.. Progress Report on Cold-Formed Steel Purlin Design. Proceedings of the third International Specialty Conference on Cold-formed Steel Structures, St Louis, Missouri, USA, 1975, 599-620.

[2] Peköz T.. Continuous Purlin Tests. Department of Structural Engineering Report, Cornell University, Ithaca, New York, 1975

[3] Peköz T.. Soroushian P.. Behaviour of C- and Z- purlins under wind uplift. Proceedings of the sixth International Specialty Conference on Cold-formed Steel Structures, St Louis, Missouri, USA, 1982, 409–429

[4] Carballo M. Strength of z-purlin supported standing seam roof systems under gravity loading. Virginia: Virginia Polytechnic Institute and State University, 1989.

[5] Brooks Steven, Murray Thomas M. Evaluation of the base test method for predicting the flexural strength of standing seam roof systems under gravity loading. Virginia: Virginia Polytechnic Institute and State University, 1989.

[6] Brooks S D, Murray T M. A method for determining the strength of Z-and C-purlin supported standing seam roof systems. Proceedings of the tenth

International Specialty Conference on Cold-formed Steel Structures, St Louis, Missouri, USA, 1990, 421-440.

[7] Anderson B B. Standing seam roof system strength under uplift loading. Virginia: Virginia Polytechnic Institute and State University, 1991.

[8] Fisher J M, Nunnery J N. Stability of standing seam roof - purlin systems. Proceedings of the thirteenth International Specialty Conference on Cold-formed Steel Structures, St Louis, Missouri, USA, 1996, 455-463.

[9] Trout A M. Further Study of the Gravity Loading Base Test Method. Virginia Polytechnic Institute and State University, 2000.

[10] NAS. AISI S100. North Amercian Specifications for the Design of Cold-Formed Steel Structural Members. AISI S100-16, American Iron and Steel Institute, Washington, D. C., 2016

[11] Technical Code of Cold-Formed Thin-Wall Steel Structures. Beijing: China Planning Press, 2002